ROYAL SOCIETY OF CHEMISTRY

Check for updates

Improvement of electronic structure calculations for the interpretation of the emission spectrum for Nd^{III} complexes†

Yolimar Gil, [ID] [a] María José Maldonado, [ID] [a] Ricardo Costa de Santana, [ID] [b] Andrés Vega, [ID] [c] Pablo Fuentealba [ID] *[a] and Daniel Aravena [ID] *[d]

A protocol to correct *ab initio* calculated luminescence spectra of Nd^{III} complexes is proposed. The emission spectrum of [Nd^{III}(bipy)(tta)$_3$] was measured to calibrate the optimal correction for the Racah parameters on top of a CASSCF calculation to attain the best energetic placement of the $^4F_{3/2} \rightarrow {}^4I_{13/2-9/2}$ emission lines. As interelectronic repulsion is the most important source of error in this calculation, this straightforward correction results in an accurate placement of transitions, allowing the assignment of a complex spectral shape in terms of its underlying transitions. Finally, the correction derived for [Nd^{III}(bipy)(tta)$_3$] was directly applied to a different Nd^{III} complex, demonstrating the broad use of this approach.

Introduction

Electronic structure calculations are extensively employed in many fields of chemistry to augment the information extractable from experimental measurements. For instance, reactivity studies can often identify products and determine information about reaction rates purely from experimental data, while detailed mechanistic proposals are often based on electronic structure calculations.[1] Similar approaches are found in other fields such as magnetism, where the overall magnetic moment can be probed experimentally but the microscopic magnetic interactions responsible for that response are studied computationally.[2] In the field of spectroscopy, *ab initio* calculations are often exploited to aid in the assignment of spectra ranging from magnetic resonances to high-energy techniques, such as X-ray experiments.[3]

UV/vis absorption and emission spectroscopy studies routinely profit from this experimental and theoretical synergy. The most common computational method in this area is time dependent density functional theory (TD-DFT),[4] which provides excitation energies and oscillator strengths at an affordable computational cost for molecular systems up to a couple hundred of atoms at the present time. In many cases, the deviations between experimental and TD-DFT predicted spectra are systematic and fixed energy shifts are used to force a better match between experiment and theory.[5] Such corrections, although empirical, have proven to be useful enough to become common practice nowadays, especially for closed shell, organic molecules.

Inorganic systems, particularly lanthanides, have their own caveats which complicate the computational production of spectra that can accurately match experiments, even employing simple empirical corrections. The most fundamental problem is the inadequacy of single reference methods, such as DFT, to provide spectroscopically consistent wave functions.[6] This can be solved using multireference methods such as complete active space self-consistent field (CASSCF), confirmed by the generalized use of this method in lanthanide magnetism.[7-15] However, CASSCF calculations suffer from additional problems to be accurate in optics. The most important is their lack of dynamical correlation, which leads to the overestimation of interelectronic repulsion, resulting in poor relative energies between 4f multiplets.[16] This effect manifests in strong misplacements of f–f absorption and emission band wavelengths, which can be as large as hundreds of nanometres. Even worse, the relative energy of each pair of multiplets will be displaced by a different magnitude in a complicated way, preventing the use of a fixed energy shift to correct the experiment. Interestingly, ligand field and spin–orbit effects are better described in lanthanide CASSCF calculations,[16] so the correction of just

[a] Facultad de Ciencias Químicas y Farmacéuticas, Universidad de Chile, Olivos 1007, 8380544 Santiago, Chile. E-mail: pfuentealbacastro@ciq.uchile.cl

[b] Instituto de Física, Universidade Federal de Goiás, Goiania 74690-900, GO, Brazil

[c] Facultad de Ciencias Exactas, Dpto. de Ciencias Químicas, Universidad Andrés Bello, Viña del Mar, Chile

[d] Departamento de Química de los Materiales, Facultad de Química y Biología, Universidad de Santiago de Chile, Casilla 40, Correo 33, Santiago, Chile. E-mail: daniel.aravena.p@usach.cl

† Electronic supplementary information (ESI) available: Additional structural and spectroscopic data, and sample input files. CCDC 2421205. For ESI and crystallographic data in CIF or other electronic format see DOI: https://doi.org/10.1039/d5cp00508f

This journal is © the Owner Societies 2025

Phys. Chem. Chem. Phys., 2025, **27**, 9847–9854 | **9847**

interelectronic repulsion can yield a dramatic correction of f–f transition energies.

Recent advances in this field indicate that a good description of lanthanide luminescence requires the calculation of larger active spaces, including additional orbital shells of the lanthanide and key ligand orbitals.[17,18] Perturbative corrections are also beneficial for a better agreement with experimental data.[19] The main drawback of this path is the increased computational cost of these more sophisticated approaches and the need for assessing the proper active space in a case to case basis.

In this article, we provide a simple procedure to correct CASSCF calculations to obtain NIR emission spectra with a good placement of the f–f bands in Nd^{III} complexes. Thus, this protocol helps in the assignment of the main features of the spectra without increasing the computational cost beyond the one associated with CASSCF. The procedure does not rely on any symmetry idealization of the coordination environment and can be thus applied to high- and low-symmetry systems at an equal footing. This correction is general for any Nd^{III} system and was calibrated using the emission spectrum of tris(thenoyl-trifluoroacetonato)2,2′-dipyridylneodymium(III) ([Nd^{III}(bipy)(tta)$_3$]), which was synthesized using literature methods[20] and measured in our laboratory. CASSCF calculations were performed using the crystallographic structure deposited in the CCDC database[21] (see Fig. 1). The faint nephelauxetic effect present in lanthanides suggests that the correction of Racah parameters derived for [Nd^{III}(bipy)(tta)$_3$] will be useful for other Nd^{III} systems without the need of recalibrating them in a case-to-case fashion. To prove this point, we synthesized a new Nd^{III} complex with a completely different coordination environment ([Nd^{III}L^1(NCS)$_3$]) (Fig. 1). Then, we measured its emission spectrum at room temperature and applied the corrected CASSCF protocol, achieving a good agreement between experimental and theoretical data.

Energy correction procedure

The procedure to generate the corrected spectrum considers three steps: (i) perform a standard CASSCF(3,7) calculation considering all quartet (35) and doublet (112) roots, where the active space includes the 4f shell of the Nd^{III} ion, (ii) obtain the corrected energies using orca_lft with the corrected Racah parameters provided in this article and (iii) perform a new CASSCF calculation using the corrected energies. The last calculation can be run on top of the converged wavefunction of the first step, so the simulation will mark convergence at the first step and proceed to the spin–orbit coupling part swiftly. A detailed example of the procedure is provided as ESI.†

The emission spectrum is simulated assuming the following formula for the intensity (I):[22–24]

$$I = \frac{4E_{if}}{3c^3\hbar^4}\left(|\boldsymbol{\mu}_{if}|^2 + |\boldsymbol{m}_{if}|^2 + |\boldsymbol{Q}_{if}|^2\right) \qquad (1)$$

where $\hbar$ is the reduced Planck constant, c is the speed of light, E_{if} is the transition energy between the initial (i) and final state (f) and $\boldsymbol{\mu}$, $\boldsymbol{m}$ and $\boldsymbol{Q}$ are the electric dipolar, magnetic dipolar and electric quadrupolar transition moments, respectively.
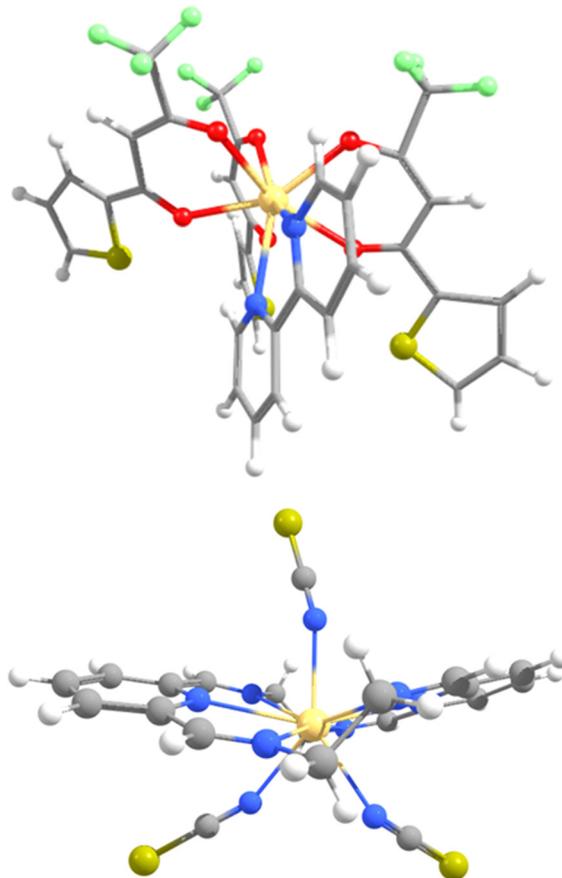

Fig. 1 Molecular structures of the [Nd^{III}(bipy)tta$_3$] (top) and [Nd^{III}L^1(NCS)$_3$] (bottom). Colour code: Nd (light yellow), S (yellow), F (light green), O (red), N (blue), C (grey) and H (white).

Our calculations indicate that magnetic dipolar and magnetic quadrupolar contributions are negligible in comparison to μ for the $^4F_{3/2} \rightarrow {}^4I_{13/2,11/2,9/2}$ transitions, as expected from Richardson's analysis of selection rules.[25]

To perform the statistical fit of the corrected Racah parameters, we synthesized a simple, yet representative emissive complex, [Nd^{III}(bipy)(tta)$_3$]. The choice of Nd^{III} is intended to provide a NIR emission spectrum with several discernible bands to fit ($^4F_{3/2} \rightarrow {}^4I_J$ (J = 9/2–13/2)). The function to optimize was the cross-correlation between the experimental and calculated emission curves. As the Nd^{III} spectrum shows three relevant NIR bands with different intensities, the cross-correlation was calculated for each peak separately, where experimental and calculated data were normalised to present a maximum of 1. Thus, the optimization function to maximize was the sum of squares of the three cross-correlations. In this way, the optimization procedure will not be biased towards adjusting the most intense peak at the expense of the other two. The maximum of the cross-correlation function was searched using the LIPO algorithm.[26] The curve broadening was chosen to maximize the objective function at each point of the optimization, so the final Racah parameters are not affected by the broadening.

9848 | *Phys. Chem. Chem. Phys.*, 2025, **27**, 9847–9854

This journal is © the Owner Societies 2025

Results and discussion

The molecular structures of $[Nd^{III}(bipy)(tta)_3]$ and $[Nd^{III}L^1(NCS)_3]$ are presented in Fig. 1, which evidences the differing coordination environment observed for these two compounds. Starting from the nature of the donor atoms, $[Nd^{III}(bipy)(tta)_3]$ exhibits an O_6N_2 motif from the three acetonates and the bipyridine ligand. In contrast, $[Nd^{III}L^1(NCS)_3]$ shows a first coordination sphere composed exclusively by nitrogen atoms.

In terms of geometrical conformation, $[Nd^{III}(bipy)(tta)_3]$ is an octacoordinated complex, which can be better described as a distorted square antiprism (with a Shape measure of 0.651). On the other hand, $[Nd^{III}L^1(NCS)_3]$ is a nonacoordinate system close to the muffin and the hula-hoop conformation (3.591 and 3.823, respectively). As discussed later, these differences were sufficient for obtaining two clearly distinguishable emission profiles for the most intense band ($^4F_{3/2} \rightarrow {}^4I_{11/2}$). In this way, we can test if the proposed correction can provide spectral shapes, which include meaningful features of the coordination environment besides the bare energy correction of the bands.

Fig. 2 presents the experimental and calculated emission spectra for $[Nd^{III}(bipy)(tta)_3]$, which served to calibrate the corrected Racah parameters, as described in the previous section. As expected, the CASSCF calculation (olive line) depicts a strong overestimation of the energy difference between the $^4F_{3/2}$ and the ^4I multiplets, resulting in a general blueshift of the bands, which is around 250–400 nm, depending on the band. The NEVPT2 corrected results (violet) shift closer to the experiment, with a slight difference for the maximum of the $^4F_{3/2} \rightarrow {}^4I_{11/2}$ transition. The CASSCF corrected spectrum (red) shows an accurate placement of the bands, consistent with the optimization procedure. The shape and relative intensity of the three bands is reasonably captured by all methods. In the case of the most intense band ($^4F_{3/2} \rightarrow {}^4I_{11/2}$), there are three discernible

peaks which descend in intensity at longer wavelength. This pattern is captured in all calculations.

Table 1 shows the comparison between the CASSCF, NEVPT2, CASSCF optimized, and experimental Racah parameters. CASSCF calculations yield a large overestimation of interelectronic repulsion, as expected by the lack of dynamical correlation characteristic of this method.[16] Perturbative approaches, such as NEVPT2 can correct for this deviation. In this case, almost matching the reference values. However, the computational burden of NEVPT2 can significantly extend the computation time of the bare CASSCF since all quartet (35) and doublet (112) roots must be corrected. In this case, the total execution time of the CASSCF run was 2 h while the NEVPT2 calculation took 237 h. The difference in execution time between NEVPT2 and CASSCF depends strongly on the number of roots to calculate. In this sense, other emissive lanthanides have an even larger number of roots (as Eu^{III} or Tb^{III}), so the computational time of NEVPT2 can be even longer. On the other side, ions like Pr^{III} and Tm^{III} have fewer roots to correct so NEVPT2 should be more accessible.

Corrected CASSCF calculations provide an accurate placement of the emission bands, close to the one obtained from NEVTP2. Thus, the statistical fit of the emission curve of $[Nd^{III}(bipy)(tta)_3]$ produced effective Hamiltonian parameters, which are close to the ones adjusted to lanthanide elpasolites in ref. 27 and 28 in accordance with the inner nature and relative insensitivity of the 4f shell with respect to the coordination environment.

After establishing the procedure and its comparison with experiments, we employed the information derived from the calculation to describe the main features of the emission spectrum for $[Nd^{III}(bipy)(tta)_3]$. Focusing on the most intense peak ($^4F_{3/2} \rightarrow {}^4I_{11/2}$), we can decompose the contributions from each Kramers' doublet to the total emission, either from the initial ($^4F_{3/2}$) or final state ($^4I_{11/2}$). The maximum splitting of $^4F_{3/2}$ and $^4I_{11/2}$ multiplets is two and six, respectively; thus, the $^4F_{3/2} \rightarrow {}^4I_{11/2}$ band can be decomposed in twelve transitions. Fig. 3 shows the decomposition of the emission stemming from the low (blue bands) and high (red bands) energy Kramers' doublets of the $^4F_{3/2}$ multiplet. Clearly, the three peak pattern is generated by the transitions from the lower energy doublet of $^4F_{3/2}$ to the six components of the $^4I_{11/2}$ multiplet, which are distributed in three main blocks involving one (1), two (2, 3) and three (4, 5, 6) Kramers' doublets (see Dieke diagram in Fig. 3).
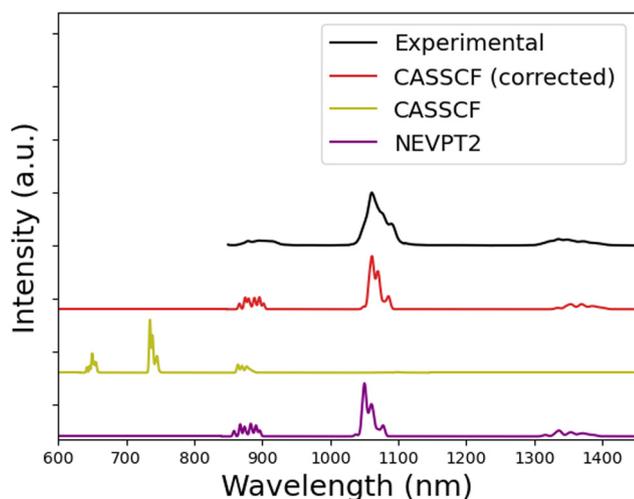

Fig. 2 Experimental (black) and calculated emission spectrum for $[Nd^{III}(bipy)(tta)_3]$ at 300 K and $\lambda_{exc} = 804$ nm. The corrected spectrum is depicted in red colour. The CASSCF and NEVPT2 spectra are presented in olive and violet colours, respectively.

Table 1 Experimental and calculated E^1, E^2 and E^3 (Racah) parameters (cm^{-1})

	E^1	E^2	E^3
CASSCF	6391.5	35.5	679.4
NEVPT2	5071.8	25.1	486.6
Optimized	5106.8	24.7	482.1
Experimental[a]	4766.5	22.6	476.5

[a] Experimental values correspond to lanthanide elpasolites and were obtained from ref. 27 and 28.

This journal is © the Owner Societies 2025

Phys. Chem. Chem. Phys., 2025, **27**, 9847–9854 | **9849**

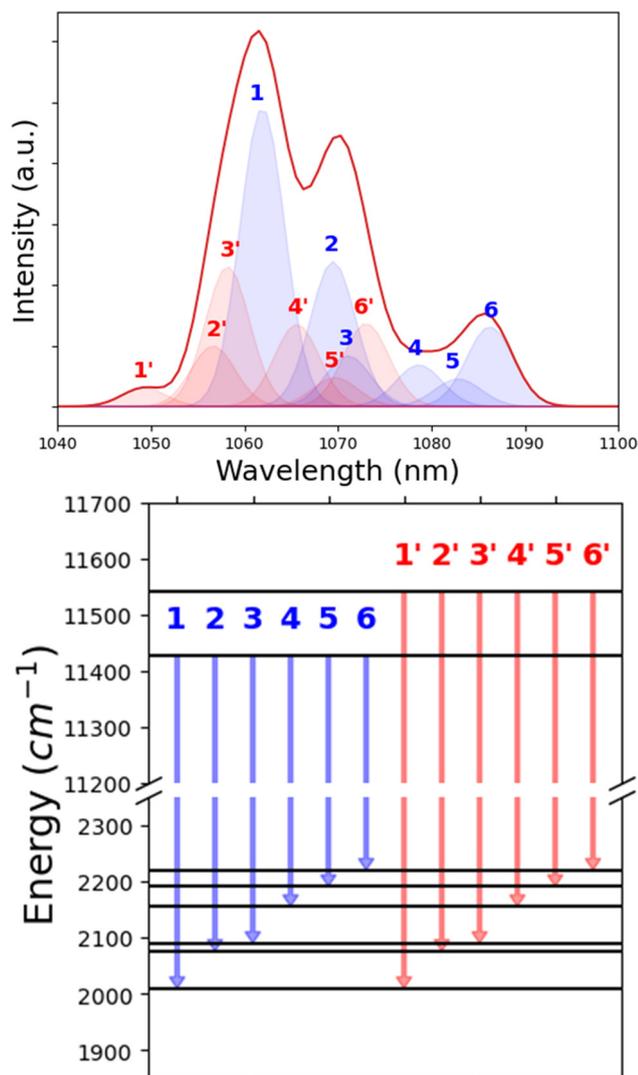Fig. 3 Top: Decomposition of the $^4F_{3/2} \rightarrow {}^4I_{11/2}$ band in the contributions of each pair of Kramers' doublets (top) and calculated Dieke diagram (bottom) for [Nd^{III}(bipy)(tta)$_3$]. Blue and red colours indicate emission stemming from the lower and upper energy doublet of the $^4F_{3/2}$ multiplet, respectively.

Fig. 4 Experimental (black) and calculated (blue) emission spectra for [Nd^{III}(bipy)(tta)$_3$] (top) and [Nd^{III}L^1(NCS)$_3$] (bottom) at 300 K and λ_{exc} = 804 nm. The molecular structures are depicted as the inset; colour code: Nd (light yellow), S (yellow), F (light green), O (red), N (blue), C (grey) and H (white). All maximum intensities were normalized to a common factor and the baseline of the calculated data was displaced for a better visualization.

The contributions from the upper doublet of $^4F_{3/2}$ mainly give intensity to the two more intense peaks and result in a weak signal at the left end of the band. In the literature, these peaks are known as hot bands,[29,30] and are indeed assigned to emission of high energy states of the emissive doublet.

To check the accuracy of the method and its applicability to other systems, we synthesized the Nd^{III} analog of a complex previously published by our group ([Nd^{III}L^1(NCS)$_3$], according to the nomenclature of ref. 31). As mentioned earlier, this complex presents a different coordination number and therefore coordination geometry than [Nd^{III}(bipy)(tta)$_3$], and the first coordination sphere is formed by only nitrogen atoms. Fig. 4 shows the satisfactory performance of the method in this new system, which even captures the different pattern observed for the main peak, with two clearly discernible maxima for
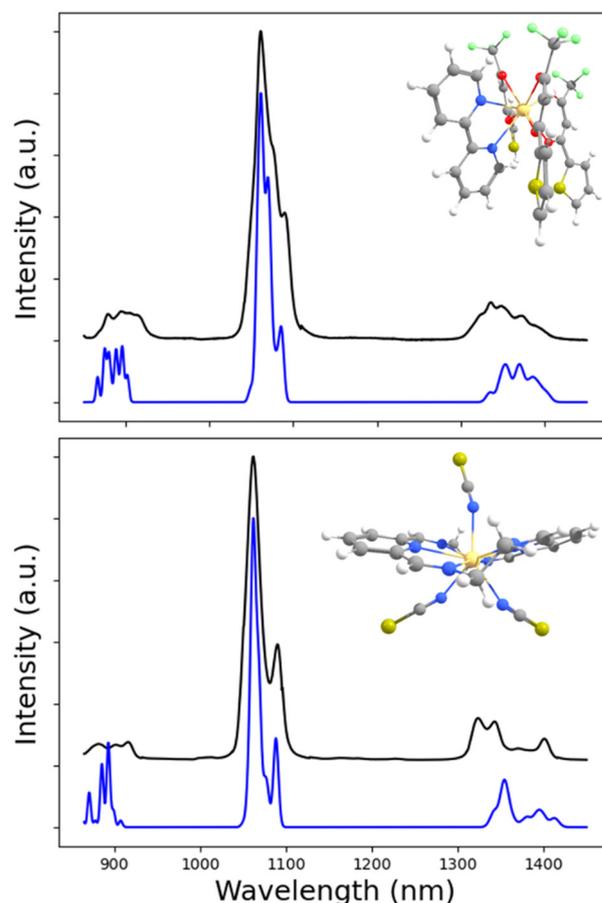
[Nd^{III}L^1(NCS)$_3$] instead of the three peaks observed for [Nd^{III}(bipy)(tta)$_3$].

As evidenced by the decomposition of the $^4F_{3/2} \rightarrow {}^4I_{11/2}$ band from [Nd^{III}L^1(NCS)$_3$], the origin of the two-peak patterns relates to a different pattern in the transition intensities in comparison to the one observed for [Nd^{III}(bipy)(tta)$_3$] (see Fig. 5). In the case of [Nd^{III}L^1(NCS)$_3$], there is a very intense transition stemming from the higher emissive Kramers' doublet, which dominates the peak at shorter wavelength (indicated as 4′ in Fig. 5). The other main peak is exclusively explained by one transition from the lower emissive state (transition 6 in Fig. 5). Hence, we can expect a different behaviour of these two peaks with respect to temperature, following the change in population of their respective emissive states. This contrasts with the situation for [Nd^{III}(bipy)(tta)$_3$], where the three peak pattern was mainly sustained by transitions associated with the lower emissive doublet.

We conclude this discussion with some general remarks about the extension of this correction for other lanthanide ions. In principle, there is no limitation to applying this same
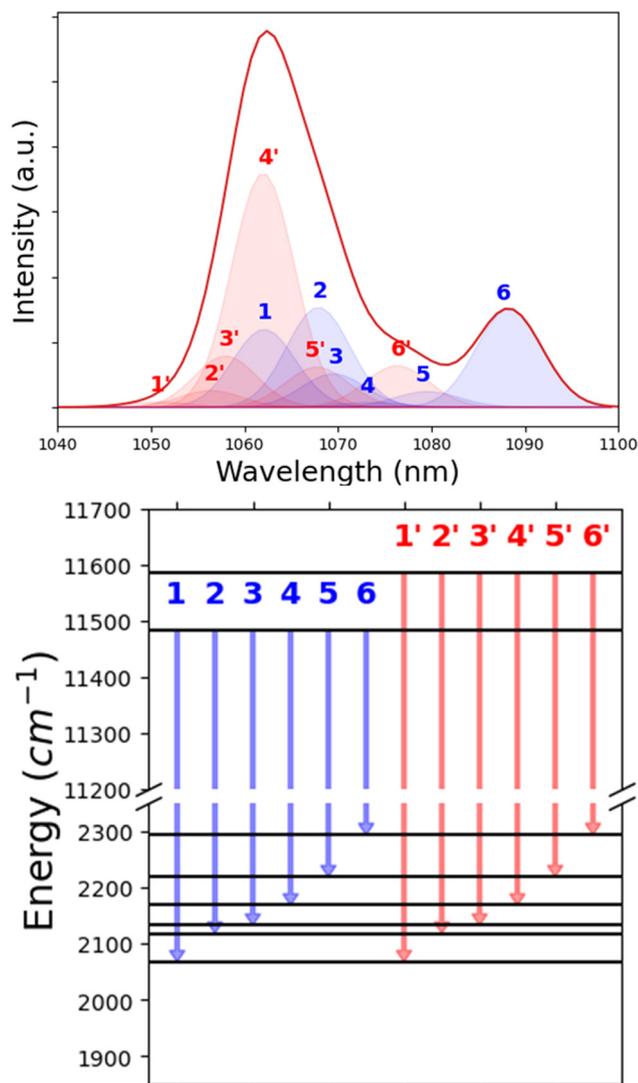
9850 | *Phys. Chem. Chem. Phys.*, 2025, **27**, 9847–9854

This journal is © the Owner Societies 2025

Fig. 5 Top: Decomposition of the $^4F_{3/2} \rightarrow {}^4I_{11/2}$ band in the contributions of each pair of Kramers' doublets (top) and calculated Dieke diagram (bottom) for [Nd^{III}L^1(NCS)$_3$]. Blue and red colours indicate emission stemming from the lower and upper energy doublet of the $^4F_{3/2}$ multiplet, respectively.

correct this bias, either by exploring more sophisticated *ab initio* methods or introducing *ad hoc* corrections.

Conclusions

In sum, we optimized Racah parameters to correct CASSCF(3,7) calculations, obtaining a better placement of the emission bands of Nd^{III} complexes. The corrected spectrum was in close agreement with reference experimental data and with NEVPT2, which is a more sophisticated and computationally demanding approach. Furthermore, the shape of the most intense peak was satisfactorily reproduced for the two studied systems. This level of agreement allowed the decomposition of the band shape into their individual contributions and the discovery of the transitions responsible for the observed pattern. In this way, the three-maxima shape for the most intense peak of [Nd^{III}(bipy)(tta)$_3$] is related with transitions originating from the lower emissive doublet of the $^4F_{3/2}$ multiplet, while the pattern of [Nd^{III}L^1(NCS)$_3$] mixes contributions from both doublets belonging to $^4F_{3/2}$. This analysis suggests a different thermal dependence of both spectroscopic signals. This kind of analysis could be useful for luminescence thermometry studies.

Experimental

Synthesis of [Nd^{III}(bipy)tta$_3$]

Reagent grade chemicals and HPLC quality solvents were used as received. The synthesis of [Nd^{III}(bipy)(tta)$_3$] was performed by using an Anton Paar microwave reactor MonoWave 200, following a reported procedure with some modifications,[20] which is described as follows: 2-thenoyltrifluoroacetone (267 mg, 1.2 mmol) and triethylamine (168 μL, 1.2 mmol) were added to a 30-mL volume microwave vial containing 15 mL of methanol:ethanol mixture (1:1). Then, Nd(NO$_3$)$_3$·6H$_2$O (175 mg, 0.4 mmol) was added and the mixture was stirred for 15 min. Finally, a solution of 2,2′-bipyridine (bipy) (63.2 mg, 0.4 mmol) in 5 mL of the same solvent mixture was added, and the resulting solution was irradiated in the microwave reactor for 15 min at 100 °C. Purple rod crystals were obtained by slow evaporation of the reaction solution after 4 days with a yield of 265 mg (69%).

Synthesis of [Nd^{III}L^1(NCS)$_3$]

To obtain the mononuclear Nd^{III} complex, the template reaction was done by reproducing a procedure that was previously published by our group,[31] which is briefly described as follows: an ethanolic solution of the lanthanide triflate salt (0.5 mmol/ 30 mL) was added to a solution of 2,6-pyridinedicarboxaldehyde (1 mmol/50 mL acetonitrile), under constant stirring at room temperature. To close the macrocyclic ligand, ethylenediamine was added dropwise (1 mmol/50 mL acetonitrile). Finally, to incorporate the thiocyanate anions, Bu$_4$NSCN was added (1.5 mmol/20 mL ethanol). The final solution was stirred for four hours, obtaining a homogeneous solution. Single crystals were formed from the mother liquor after two or three weeks (42.7% yield).

optimization procedure to spectra for other lanthanides. However, the optimization of the spectral shape requires that the source CASSCF calculation can produce transition intensities that resemble the experimental pattern to provide a meaningful fit. This is the case for [Nd^{III}(bipy)(tta)$_3$] and [Nd^{III}L^1(NCS)$_3$], where the three and two peak patterns for the most intense transition are reproduced in the bare CASSCF calculations, even if they are strongly misplaced in energy. This situation is not expected to be generally extensible for other lanthanide ions, especially for transitions with mixed electric and magnetic dipole mechanisms. In such situations, CASSCF will probably capture the intensity of the magnetic term properly, but will strongly underestimate the electric term. As both contributions follow different patterns, the calculated shape will not follow the observed trend. Thus, it is necessary to develop a method to

This journal is © the Owner Societies 2025

Phys. Chem. Chem. Phys., 2025, **27**, 9847–9854 | **9851**

Structural and spectroscopic characterization

Powder X-ray diffraction (PXRD) patterns were collected at room temperature using Bruker D-8 ADVANCE equipment, with CuKα1 radiation. This pattern was compared with the calculated PXRD obtained from the crystal structure[32] (Fig. S1, ESI†). The agreement of these patterns supports the pure state of the bulk. The solid-state emission spectrum was recorded on a spectrofluorimeter (Fluorolog-3, Horiba Scientific) with a diode laser (Crystal Laser LC) of 804 nm.

Computational details

All calculations were carried out using the ORCA 5.0.4 software.[33,34] As the crystal structure of $[Nd^{III}(bipy)(tta)_3]$ from the CCDC database[21] lacked hydrogen atoms and presented disorder at the thiophene groups, a geometry optimization of the peripheral atoms was performed prior to the CASSCF calculations. To avoid disrupting the coordination environment of the Nd^{III} ion, the metal position, all coordinating atoms and carbon atoms forming the chelate bite were kept frozen at their crystallographic positions. To avoid convergence problems, the Nd^{III} ion was replaced by Y^{III}. The structural relaxation was done by a density functional theory calculation using the BP86 functional[35,36] and the Def2-TZVP basis set,[37] including a 28 electron ECP for the Y atom.[38] The crystallographic structure of $[NdL^1(NCS)_3]$ was employed without further optimization. CASSCF(3,7)[39] calculations were run on top of the optimized structure, where the active space was composed of the 4f electrons. 35 quartets and 112 doublets were considered to saturate the excitation space. The Def2-TZVP basis set was selected for light elements and the SARC2-DKH-QZVP[40] basis set was chosen for Nd^{III}. NEVPT2[19,41,42] correction was applied on top of the CASSCF converged wave functions. Racah, spin–orbit coupling and ligand field parameters were obtained by means of the *ab initio* ligand field theory approach.[43] Scalar relativistic effects were accounted for using the DKH Hamiltonian.[44,45] Spin–orbit coupling was described by means of the Quasi-degenerate perturbation theory. Calculations were accelerated by using the RI approximation for the integral transformation step.[46]

Magnetic dipole and electric quadrupole contributions were calculated using the "quad true" keyword although they were later discarded from the analysis since their magnitude was negligible in comparison to the electric dipole term. The emission spectrum was calculated by extracting the oscillator strength from the absorption spectrum and weighting the population of the emissive $^4F_{3/2}$ multiplet by their Boltzmann population. The intensity is calculated as in eqn (1).[22–24]

Author contributions

Yolimar Gil: investigation, data curation, writing; María José Maldonado: investigation, data curation.; Ricardo Costa de Santana: resources, writing; Andrés Vega: investigation, data curation, writing; Pablo Fuentealba: investigation, data curation, writing; Daniel Aravena: conceptualization, investigation, formal analysis, writing.

Data availability

The data supporting this article have been included as part of the ESI.† The crystal structure of $[Nd^{III}L^1(NCS)_3]$ was deposited with the CCDC number 2421205.

Conflicts of interest

There are no conflicts to declare.

Acknowledgements

References

1 M. Breugst, *Enabling Tools and Techniques for Organic Synthesis*, Wiley, 2023, pp. 259–311.

2 G. Rajaraman, *Computational Modelling of Molecular Nanomagnets*, Springer International Publishing, Cham, 2023, vol. 34.

3 V. Barone, S. Alessandrini, M. Biczysko, J. R. Cheeseman, D. C. Clary, A. B. McCoy, R. J. DiRisio, F. Neese, M. Melosso and C. Puzzarini, Computational molecular spectroscopy, *Nat. Rev. Methods Primers*, 2021, **1**, 38.

4 E. Runge and E. K. U. Gross, Density-Functional Theory for Time-Dependent Systems, *Phys. Rev. Lett.*, 1984, **52**, 997–1000.

5 A. Ali, M. I. Rafiq, Z. Zhang, J. Cao, R. Geng, B. Zhou and W. Tang, TD-DFT benchmark for UV-visible spectra of fused-ring electron acceptors using global and range-separated hybrids, *Phys. Chem. Chem. Phys.*, 2020, **22**, 7864–7874.

6 F. Neese, Prediction of molecular properties and molecular spectroscopy with density functional theory: From fundamental theory to exchange-coupling, *Coord. Chem. Rev.*, 2009, **253**, 526–563.

7 Y. Gil and D. Aravena, Understanding Single-Molecule Magnet properties of lanthanide complexes from 4f orbital splitting, *Dalton Trans.*, 2024, **53**, 2207–2217.

8 J. Torrent, C. Puigjaner, R. Herchel and J. Mayans, Cerium-Based Metal–Organic Frameworks: Unveiling the Role of Terahertz Vibrations in the Spin Relaxation Dynamics, *Inorg. Chem.*, 2025, **64**, 3735–3746.

9 V. Briganti and A. Lunghi, A machine-learning framework for accelerating spin-lattice relaxation simulations, *NPJ Comput. Mater.*, 2025, **11**, 62.

10 X. Gou, Y. Wu, H. Wen, L. Li, W. Lan, N. Liu, S. Zhang, L. Ungur, P. Cheng and W. Shi, Modulating Static and Dynamic Magnetizations of Ytterbium(III) Coordination Polymers by Light-Induced Radicals, CCS, *Chemistry*, 2025, 1–9.

9852 | *Phys. Chem. Chem. Phys.*, 2025, **27**, 9847–9854

This journal is © the Owner Societies 2025

11 V. Vieru, S. Gómez-Coca, E. Ruiz and L. F. Chibotaru, Increasing the Magnetic Blocking Temperature of Single-Molecule Magnets, *Angew. Chem., Int. Ed. Engl.*, 2024, **63**, e202303146.

12 À. Tubau, S. Gómez-Coca, S. Speed, M. Font-Bardía and R. Vicente, New series of mononuclear β-diketonate cerium(III) field induced single-molecule magnets, *Dalton Trans.*, 2024, **53**, 9387–9405.

13 S. C. Corner, G. K. Gransbury, I. J. Vitorica-Yrezabal, G. F. S. Whitehead, N. F. Chilton and D. P. Mills, Halobenzene Adducts of a Dysprosocenium Single-Molecule Magnet, *Inorg. Chem.*, 2024, **63**, 9552–9561.

14 A. Swain, Y. L. Whyatt, D. Wielechowski, S. Muthu, S. L. Benjamin, K. S. Murray, G. Rajaraman and S. K. Langley, Enhancing blocking temperatures in {$Cr^{III}_2Dy^{III}_2$} butterfly SMMs: deciphering the role of exchange interactions and developing magneto-structural maps, *Inorg. Chem. Front.*, 2025, **12**, 1059–1079.

15 N. Monni, S. Dey, V. García-López, M. Oggianu, J. J. Baldoví, M. L. Mercuri, M. Clemente-León and E. Coronado, Tunable SIM properties in a family of 3D anilato-based lanthanide-MOFs, *Inorg. Chem. Front.*, 2024, **11**, 5913–5923.

16 D. Aravena, M. Atanasov and F. Neese, Periodic Trends in Lanthanide Compounds through the Eyes of Multireference ab Initio Theory, *Inorg. Chem.*, 2016, **55**, 4457–4469.

17 V. R. M. Nielsen, M. Grasser, S. S. Mortensen, B. Le Guennic and T. J. Sørensen, Electronic Structure of a Neodymium(III) Tris(oxidiacetate) Complex from Luminescence Data and Ab Initio Calculations, *Inorg. Chem.*, 2024, **63**, 18596–18607.

18 M. Grasser and B. Le Guennic, Ab initio investigations of circularly polarised luminescence in Samarium(III)-based complexes, *Phys. Chem. Chem. Phys.*, 2024, **26**, 7203–7210.

19 C. Angeli, R. Cimiraglia and J.-P. Malrieu, N-electron valence state perturbation theory: a fast implementation of the strongly contracted variant, *Chem. Phys. Lett.*, 2001, **350**, 297–305.

20 H.-Y. Wong, W.-S. Lo, W. T. K. Chan and G.-L. Law, Mechanistic Investigation of Inducing Triboluminescence in Lanthanide(III) β-Diketonate Complexes, *Inorg. Chem.*, 2017, **56**, 5135–5140.

21 C. R. Groom, I. J. Bruno, M. P. Lightfoot and S. C. Ward, The Cambridge Structural Database, *Acta Crystallogr., Sect. B: Struct. Sci., Cryst. Eng. Mater.*, 2016, **72**, 171–179.

22 F. Gendron, B. Moore, O. Cador, F. Pointillart, J. Autschbach and B. Le Guennic, Ab Initio Study of Circular Dichroism and Circularly Polarized Luminescence of Spin-Allowed and Spin-Forbidden Transitions: From Organic Ketones to Lanthanide Complexes, *J. Chem. Theory Comput.*, 2019, **15**, 4140–4155.

23 B. Pritchard and J. Autschbach, Calculation of the Vibrationally Resolved, Circularly Polarized Luminescence of D-Camphorquinone and (S,S)-*trans*-β-Hydrindanone, *Chem. Phys. Chem.*, 2010, **11**, 2409–2415.

24 G. Longhi, E. Castiglioni, S. Abbate, F. Lebon and D. A. Lightner, Experimental and Calculated CPL Spectra and Related Spectroscopic Data of Camphor and Other Simple Chiral Bicyclic Ketones, *Chirality*, 2013, **25**, 589–599.

25 F. S. Richardson, Selection rules for lanthanide optical activity, *Inorg. Chem.*, 1980, **19**, 2806–2812.

26 C. Malherbe and N. Vayatis, Proceedings of the 34th International Conference on Machine Learning, 2017, vol. 70, pp. 2314–2323.

27 F. S. Richardson, M. F. Reid, J. J. Dallara and R. D. Smith, Energy levels of lanthanide ions in the cubic Cs_2NaLnC_{16} and Cs_2NaYCl_6:Ln^{3+} (doped) systems, *J. Chem. Phys.*, 1985, **83**, 3813–3830.

28 M. F. Reid and F. S. Richardson, Free-ion, crystal-field, and spin-correlated crystal-field parameters for lanthanide ions in $Cs_2NaLnCl_6$ and Cs_2NaYCl_6:Ln^{3+} systems, *J. Chem. Phys.*, 1985, **83**, 3831–3836.

29 W. Yang, M. Rosenkranz, G. Velkos, F. Ziegs, V. Dubrovin, S. Schiemenz, L. Spree, M. F. de Souza Barbosa, C. Guillemard, M. Valvidares, B. Büchner, F. Liu, S. M. Avdoshenko and A. A. Popov, Covalency versus magnetic axiality in Nd molecular magnets: Nd-photoluminescence, strong ligand-field, and unprecedented nephelauxetic effect in fullerenes $NdM_2N@C_{80}$ (M = Sc, Lu, Y), *Chem. Sci.*, 2024, **15**, 2141–2157.

30 D. K. Sardar and R. M. Yow, Stark components of $^4F_{3/2}$, $^4I_{9/2}$ and $^4I_{11/2}$ manifold energy levels and effects of temperature on the laser transition of Nd^{3+} in YVO_4, *Opt. Mater.*, 2000, **14**, 5–11.

31 Y. Gil, P. Fuentealba, A. Vega, E. Spodine and D. Aravena, Control of magnetic anisotropy by macrocyclic ligand distortion in a family of Dy^{III} and Er^{III} single molecule magnets, *Dalton Trans.*, 2020, **49**, 17709–17718.

32 J. G. Leipoldt, L. D. C. Bok, S. S. Basson and A. E. Laubscher, The crystal structure of tris(thenoyltrifluoroacetonato)2,2′-dipyridylneodymium(III), *J. Inorg. Nucl. Chem.*, 1976, **38**, 1477–1479.

33 F. Neese, Software update: The ORCA program system—Version 5.0, *WIREs Comput. Mol. Sci.*, 2022, **12**, e1606.

34 F. Neese, The SHARK integral generation and digestion system, *J. Comput. Chem.*, 2023, **44**, 381–396.

35 A. D. Becke, Density-functional exchange-energy approximation with correct asymptotic behavior, *Phys. Rev. A*, 1988, **38**, 3098–3100.

36 J. P. Perdew, Density-functional approximation for the correlation energy of the inhomogeneous electron gas, *Phys. Rev. B: Condens. Matter Mater. Phys.*, 1986, **33**, 8822–8824.

37 F. Weigend and R. Ahlrichs, Balanced basis sets of split valence, triple zeta valence and quadruple zeta valence quality for H to Rn: Design and assessment of accuracy, *Phys. Chem. Chem. Phys.*, 2005, **7**, 3297.

38 D. Andrae, U. Häussermann, M. Dolg, H. Stoll and H. Preuss, Energy-adjusted ab initio pseudopotentials for the second and third row transition elements, *Theor. Chim. Acta*, 1990, **77**, 123–141.

39 P.-Å. Malmqvist and B. O. Roos, The CASSCF state interaction method, *Chem. Phys. Lett.*, 1989, **155**, 189–194.

40 D. Aravena, F. Neese and D. A. Pantazis, Improved Segmented All-Electron Relativistically Contracted Basis Sets for the Lanthanides, *J. Chem. Theory Comput.*, 2016, **12**, 1148–1156.

41 Y. Guo, K. Sivalingam, E. F. Valeev and F. Neese, Sparse-Maps—A systematic infrastructure for reduced-scaling

This journal is © the Owner Societies 2025

Phys. Chem. Chem. Phys., 2025, **27**, 9847–9854 | 9853

electronic structure methods. III. Linear-scaling multireference domain-based pair natural orbital N-electron valence perturbation theory, *J. Chem. Phys.*, 2016, **144**, 094111.

42 C. Angeli, R. Cimiraglia, S. Evangelisti, T. Leininger and J.-P. Malrieu, Introduction of n-electron valence states for multireference perturbation theory, *J. Chem. Phys.*, 2001, **114**, 10252–10264.

43 M. Atanasov, D. Ganyushin, K. Sivalingam and F. Neese, A Modern First-Principles View on Ligand Field Theory Through the Eyes of Correlated Multireference Wavefunctions, *Molecular Electronic Structures of Transition Metal Complexes II,* Structure and Bonding, Springer, 2011, vol. 143, pp. 149–220, DOI: **10.1007/430_2011_57**.

44 M. Reiher, Douglas–Kroll–Hess Theory: a relativistic electrons-only theory for chemistry, *Theor. Chem. Acc.*, 2006, **116**, 241–252.

45 T. Nakajima and K. Hirao, The Douglas–Kroll–Hess Approach, *Chem. Rev.*, 2012, **112**, 385–402.

46 G. L. Stoychev, A. A. Auer and F. Neese, Automatic Generation of Auxiliary Basis Sets, *J. Chem. Theory Comput.*, 2017, **13**, 554–562.